Genetic Algorithm Controlled Move on Sensing Automatic Manipulation for Growing Simulation of Differentiated iPS Cells

Shintaro ISHIYAMA[*1], Mamoru MINAMI[2]

[1]Japan Atomic Energy Agency, 319-1195 Ibaragi pref. Naka-gun Tokai-mura Shirakata Shirane 2-4, Japan

[2]Graduate School of Natural Science and technology 3-1-1, Tsushimanaka, Kitaku, Okayama 700-8530, Japan

[*1]ishiyama.shintaro@jaea.go.jp; [2]sminami-m@cc.okayama-u.ac.jp

***Abstract*-A new control scheme "Move on Sensing" technology was proposed and demonstrated its great potential as an autonomous control system to respond to interaction with growing simulation environment of differentiated Induced Pluripotent Stem (iPS) cell and the following results were derived; (1) Remove of the targeted cell models was completed by 20 times selection process from original cell group model composed of 20 red and 20 blue colored beads within 16sec per cell. (2) High-accuracy sorting operation of iPS cell model was achieved within 16sec per cell. (3)Retrievability of the discrete cell models isolated from group model was ensured by use of the MOS control.**

Keywords- Visual Servoing; Move on Sensing Control; iPS Cell; Genetic Algorithm

I. INTRODUCTION

Peculiar research on stem cell and a stem cell-derived therapy are reported and lead to positive results, where inducting method of induced pluripotent stem (iPS) cells of mouse [1], and generation of iPS cells using protein [2] and iPS cells' competency [3] have been reported, and reprogramming of fibroblasts and their characters are examined [4, 5].

Recently it is proposed to apply these technologies to make up for lost organs due to diseases, accidents, etc. by cellular structure grown by iPS cells as regeneration medicine. In this regeneration medicine, stem cell which becomes in various organs, skin and tooth, assumes an important role and many scientist have been challenging the initializing and growth of stem cell to obtain objective organs. In these growing processes of iPS, stem cells grow by dividing into target cells and nontarget cells as shown in Fig. 1.

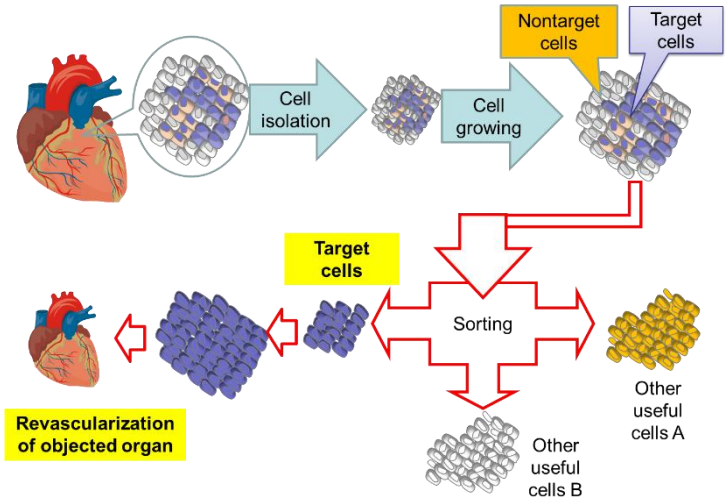

Fig. 1 Concept of cell sorting process for revascularization therapy

To obtain curative organs and tissues, sorting operation of the target cell from indifferent cells is inevitable and a huge amount of sorting works is requested. Therefore, automatic sorting machines and robots will be requested under aseptic condition for a long time operation later on. Recently, cell sorting technique and devices have been invented to handle the problem of responding to these demands, but cells are too sensitive to the oppression during device operation and results in a low survival rate after sorting. Therefore, delicate and high-precision handling techniques of cells are required for cell sorting robot systems. Main compatibility conditions demanded for these robotics are,①Recognition action of the targeted cells, ② protection algorism against damage of cells during sorting action, ③re-realization of the targeted cells in random order and disturbance generation during expansion through cell division and sorting actions.

Robots were generally designed to achieve high quality of products and minimize defective units, but its handling actions

are only permitted under very limited and predefined/non-time-varying process conditions. These limitations of robot design cause impracticability to adapt to environmental changes, including such growing environment of iPS cells.

To solve these problems, visual servoing control method [6] and image based control system [7] and visual feedback method [8] were proposed, and recently, Minami and et al. [9-11], proposed 1-step genetic algorithm (1-step GA) and demonstrated high speed recognition of the object motion and position with time-varying image processing managed by GA [12],[13].

The authors newly proposed an artificial intelligence engine, "Move on Sensing (MOS)," which is created by the combination with visual servoing and adoptive manipulation technology. The MOS programmed sorting robot system is applicable for eradicating individual cell or colonies that are uselessly proliferated, then cultivating target iPS cells selectively to make target organs.

In present paper, we conducted cell sorting simulation using the MOS programmed visual servoing robot and demonstrate sorting effectiveness by MOS technology.

II. COGNITIVE METHOD FOR THE OBJECTS OF ARBITRARY SHAPES

A. Definition of Correlated Function between Arbitrary Shaped Objective and Ellipsoidal Model

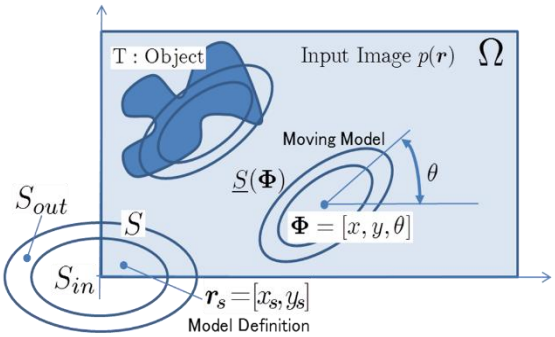

Fig. 2 Definition of moving model composed of inner-surface and outer-striper, used for detecting unknow arbitrary-sahper target

Fig. 2 shows ellipsoidal model applied for recognition of the irregular shaped objectives in present study. This model was built on the concept of model base matching method. Where, S_{in} is expressed as a whole series of points located in the ellipsoidal model and the center of S is correspondent to the origin of coordinate system. Here, long and short axis direction of the ellipsoidal model is correspondent to *x* and *y* axis, respectively. S is composed of inner ellipsoidal S_{in}, and S_{out}, which put a girdle round S_{in}. T in Fig. 2 is perceived object.

The Ω is input image region and expressed by the distribution of brightness value. Here, r_s is given by the coordinate point $[x_s,y_s]$ in S region and S and the moving ellipsoidal model S(Φ) are expressed by translation [x,y] and Φ=[x,y,θ], respectively, where θ is rotation. Point r including a whole series of points located in the moving ellipsoidal model S and a girdle round Sin is a function of Φ and r_s and expressed as:

$$\boldsymbol{r}(\boldsymbol{\Phi}, \boldsymbol{r}_S) = \begin{bmatrix} \cos\theta & -\sin\theta \\ \sin\theta & \cos\theta \end{bmatrix} \begin{bmatrix} x_S \\ y_S \end{bmatrix} + \begin{bmatrix} x \\ y \end{bmatrix} \tag{1}$$

The correlated function $\mathbf{F}(\boldsymbol{\Phi})$ is defined as:

$$\mathrm{F}(\boldsymbol{\Phi}) = \int_{\mathrm{r}\in\Omega\cap\underline{\mathrm{S}}} \mathbf{p}(\mathbf{r})\mathbf{m}(\mathbf{r})\,\mathrm{ds} \tag{2}$$

where $\mathbf{m}(\mathbf{r})$ and $\mathbf{p}(\mathbf{r})$ are the evaluation factor and the distribution of brightness values in minimal areas, respectively, element ds and the discretized m is given as:

$$\mathrm{m}(\boldsymbol{r}(\boldsymbol{\Phi}, \mathbf{r}_s)) = \begin{cases} +1 & (\boldsymbol{r}_s \in \mathrm{S}_{in}) \\ -1 & (\boldsymbol{r}_s \in \mathrm{S}_{out}) \end{cases} \tag{3}$$

From Eq. (3), Eq. (2) is re-expressed as:

$$\mathrm{F}(\boldsymbol{\Phi}) = \frac{1}{\mathrm{NM}}\{ \sum_{\boldsymbol{r}_{i,j}\in\boldsymbol{S}_{in}} \mathrm{p}(\boldsymbol{r}_{i,j}) - \sum_{\boldsymbol{r}_{i,j}\in\boldsymbol{S}_{out}} \mathrm{p}(\boldsymbol{r}_{i,j}) \} \tag{4}$$

where M is total number of searching point $\mathbf{r_s}$ in $\mathbf{S_{in}}$ and N is the maximum brightness value and normally given 0.3 as empirical value[11]. The factor $\boldsymbol{\Phi}$ concerning the position and shape of arbitrary orientation objects can be obtained as the

value which give the maximum value to $\mathbf{F}(\mathbf{\Phi})$ in global optimum solution. Suzuki et al. [12] pointed out dangerous misperception of local minimum or maximum values in multiple peaked function $\mathbf{\Phi}$ as global optimum solution from noisy vision, and the initialization method influenced an optimum solution [14, 15].

B. Detection Procedure for the Recognition of Position, Shape and Color of Arbitrary Object upon Model-Based Matching and GA Method

It is difficult to determine optimum value in the distribution in global sphere with multi peaks, since the optimization process is disturbed by hindrances of local maxima as shown in Fig.22 whose peaks mean blue beads representing nontarget cells. There is no mathematical optimization method to guarantee the convergence to find optimum solution, $\mathbf{\Phi}$, to maximize $\mathbf{F}(\mathbf{\Phi})$ in a global field with multi peaks. The optimum solution $\mathbf{\Phi}$ represents the nontarget sell position in this research. Because GA is a practical method to optimize in a field with multi-peaks through its regeneration procedures of populations by evolving process with mutation, and it has no restrictions or assumptions when applying GA for solving optimization problems.

In the 1-step GA method[12, 13], genetically optimized offspring $\mathbf{\Phi_i}(\mathbf{i}=1,2,\ldots,s)$, which gives higher $\mathbf{F}(\mathbf{\Phi_i})$, alters the tide of generational change and reaches to the global optimum solution $\mathbf{\Phi}(t)$ in time-dependent distribution function $F(\mathbf{\Phi}(t))$. This method have some features by robust stability against image noise and illuminance reduction, because this method adopts the correlation-based search for the position and motion of the objects between original image and model without any image processing. Fig.22 shows the distribution of correlation function used as fitness function in GA process---indicating every blue bead has peak and red beads have no peak---, which means GA optimization process can surely find blue beads. Further the illuminance change influence only to the height of the peaks then the GA's optimization process becomes immune to illuminance changing. This is a fruit of not using binarization of the input images.

III. EXPERIMENTAL PROCUDRE

A. Cell Group Model for Individual Cell Selection

Differential proliferation process is modeled as shown in Fig. 3 (a). This model is consisted of 20 target red and 20 nontarget blue colored plastic beads (1mm diameter with 0.1g) blending in petri dish. Here, red beads represent target iPS cells (actual size of the cell is ϕ 20-30μm), and blue beads represent nontarget cells, respectively. The task of MOS robot is to remove completely nontarget blue beads. Each bead is released from restriction but stationary if no external force exerts. When the MOS robot happens to touch the adjacent beads next to the nontarget blue bead during removing operations, the cells moves unpredictably.

B. MOS Visual Servoing Robot and Individual Cell Selection

Fig. 3(b) shows visual servoing robot (MITSUMISHI heavy industry, 7 rink typed robot, PA-10AARM ,model PA10A-300- 0045) with hand eye camera (SONY, FCB-LX11A, 38,000 pixel, view angle 46 °±5) and single cell sorting device (metal bar 10φmm with adhesion tape on the top of bar). Hand eye camera is placed on vertically-arranged robot and takes image of objects, shown in Fig. 3(c).

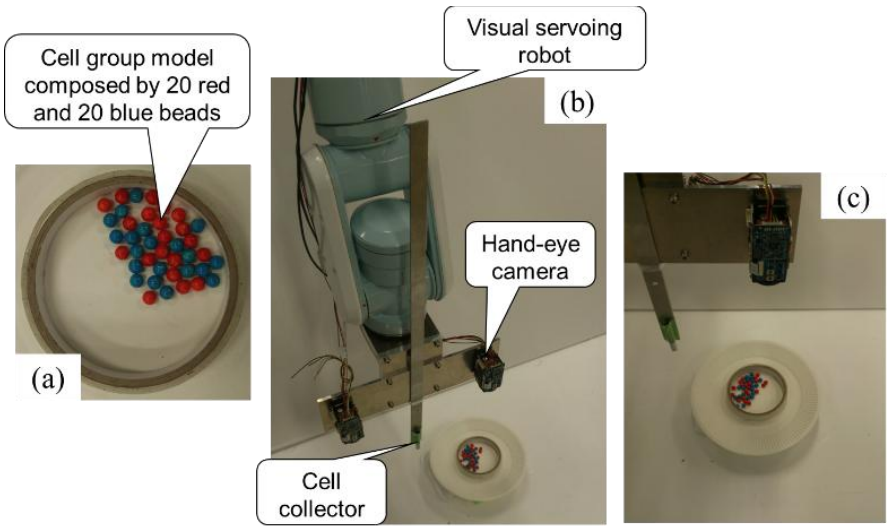

Fig. 3 Cell group model and visual servoing robot mounted hand eye camera and cell collector; (a) cell group model, (b) visual servoing robot and (c) hand-eye camera mounted on the robot

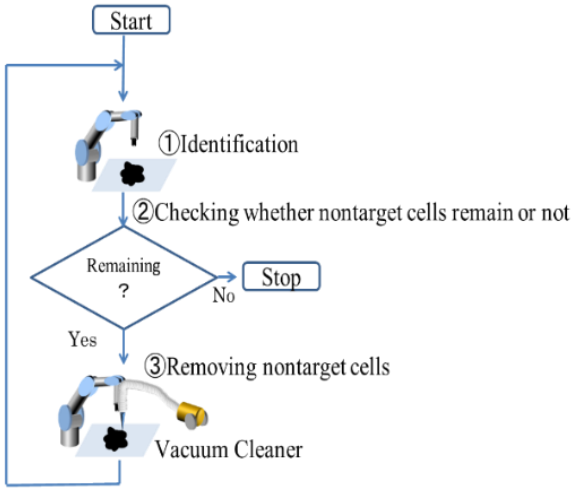

Fig. 4 Flow chart fpr removing nontarget cells including: ①IIdentification of target cells and nontarget cells, ②Checking whether nontarget cells remain or not, ③Removing nontarget cells by vacuum cleaner

C. Procedure of Individual Cell Selection

Fig. 4 shows the procedure of single cell sorting operation by the MOS robot. The MOS robot recognizes nontarget blue beads at every run represented by the loop including ①identification, ②checking, ③removing. Process ① is identification process of moving position, shape and condition(color) of the objects by ellipsoidal model, and the MOS robot distinct between target cell and nontarget cell (non-iPS cell) by the level depth of correlation $F(\Phi) > 0.7$ in process ②. Normally, the level depth of correlation more than 0.5 is thought to be enough to robot control as empirical value [6, 9-12]. The value, $F(\Phi)$, indicates how much the GA process evaluated the nontarget blue cell, then if $F(\Phi)$ satisfies a threshold of $F(\Phi) > 0.7$, then GA process determine that there is a nontarget blue cell at the position of Φ in process ②.

The Camera position was set at 300mm height from the cells group model. The sorting of the target cell models was conducted from the cell group model by making top of rod with adhesive tape contacted and attached to nontarget blue cells to remove them in process ③. This process loop ① to ③ was repeated until the nontarget blue cells are removed completely.

IV. RESULTS

Single cell sorting experiment starts with original cell group model with target 20 red and nontarget 20 blue colored beads in petri dish. 21 runs of selection operation is conducted in the experiment and red color beads are added to the petri dish by 5 beads after 5th, 10th and 15th runs, which emulates proliferations of target red iPS cells. Here, cell group models at each these stage, are defined original, 2nd, 3rd and 4th generation groups.

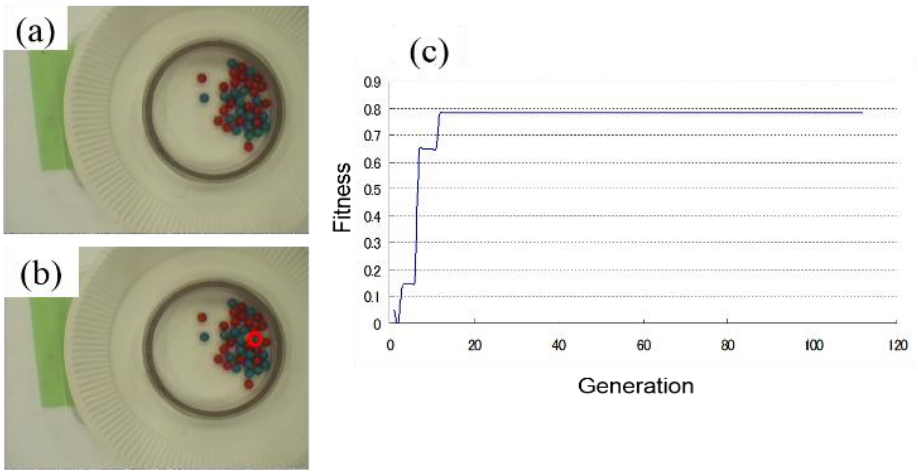

Fig. 6 The results of 4th recognition of the objected cell model in original cell group model: (a) Photo images of before and (b) after recognition and (c) convergence process of recongnition

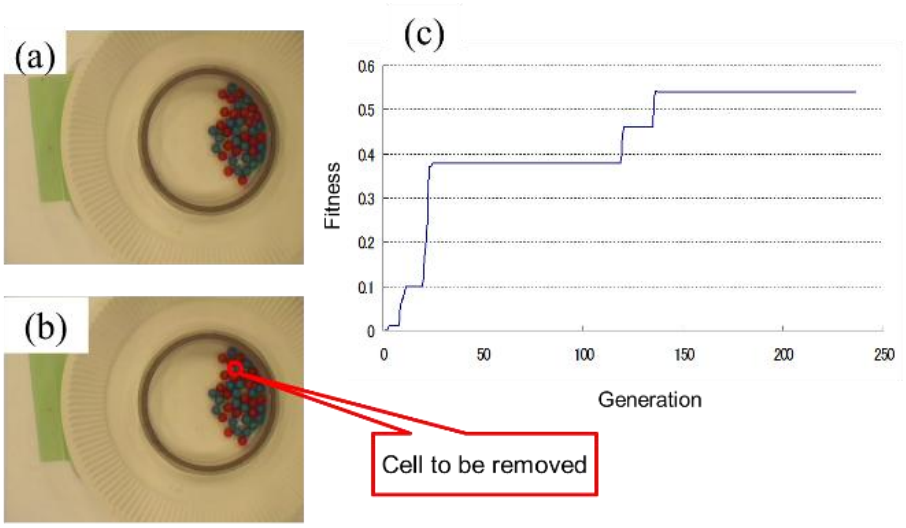

Fig. 5 The result of first recognition of objected cell model in original cell group model (a) Photo images of before, and (b) after recognition, and (c) convergence process of recognition

A. Recognition of the Targeted Single Cell Model for Original Generation Group

Fig. 5 shows first recognition results of original cell group model. Fig. 5(a) is a photo of the original cell group before recognition and Fig. 5(b) is the same photo of (a) with a red circle indicating that MOS robot plans to pick up the bead, where the position of the blue bead is identified by GA's optimization process.

The targeted single cell model of blue colored bead is located at upper part of the original cell group and set about with other red and blue colored beads. Fig. 5(c) shows the convergence process of fitness function F(Φ) with evolution cycles. It is clear that drastic convergence process steps are observed at early and final evolutionary stages and high level of convergence is achieved after 100 times trials, which means GA's optimization process has been completed.

Fourth recognition result is shown in Figs. 6(a) and (b). Rapid progress toward decentralization and arbitrary was found after first sorting by the MOS robot in original cell group model. The targeted single cell model recognized as blue colored bead by GA method presents with red circles in the figure and located in the middle of the cell group model. Higher level of convergence was achieved after less than 20 times trials with two step jump of convergence in Fig. 6(c).

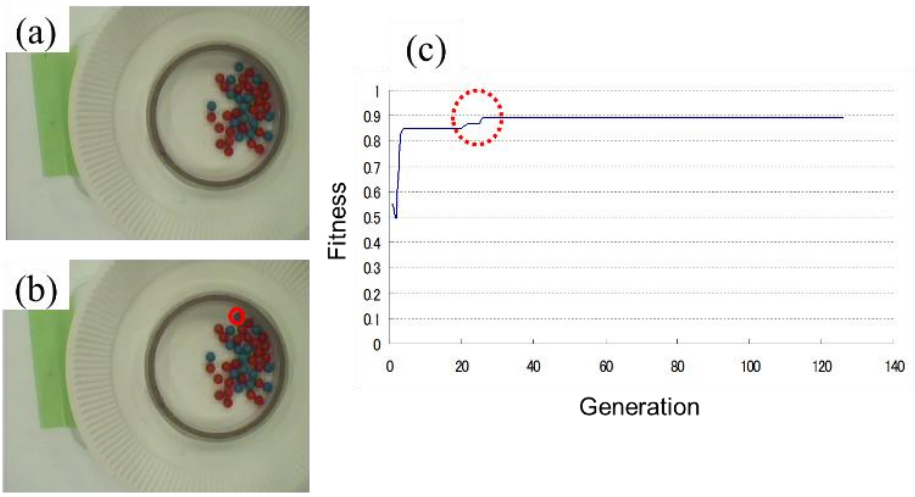

Fig. 7 The results of 6th recognition of the objected cell model in original cell group model: (a) Photo images of before, and (b) after recognition, and (c) convergence process of recognition

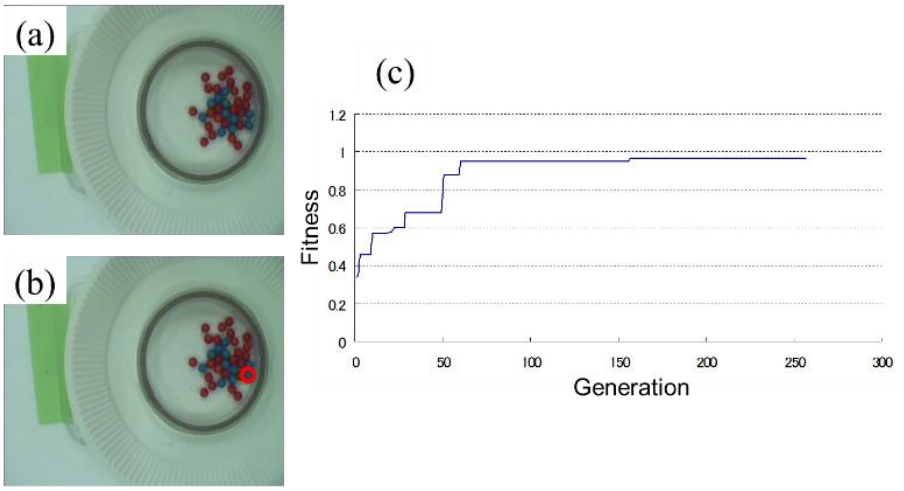

Fig. 8 The results of 10th recognition of the objected cell model in original cell group model: (a) Photo images of before, and (b) after recognition, and (c) convergence process of recognition

B. Recognition of the Targeted Single Cell Model for 2nd Generation Group

Fig. 7 shows 6th recognition results of 2nd generation cell group model. Fig. 6(a) is a photo of 2nd generation cell group model before recognition. Rapid progress toward decentralization and arbitrary was found after recharge of red colored beads into original cell group model. Fig. 7(b) is a photo after recognition.

Red colored circle presents the targeted single cell model of blue colored cell model, and the position of the target single cell model of blue colored bead is located at upper part of the original cell group and closer to the wall of petri dish in isolation. Fig. 7(c) shows the convergence process of fitness function F(Φ) with evolution cycles. Drastic convergence process steps were observed at early evolutionary stage and high level of convergence was achieved after 40 times trials. The 10th recognition result is shown in Figs. 8(a) and (b). Rapid progress toward decentralization and arbitrary was also found after 9th sorting and re-charged red beads in original cell group model. The targeted single cell model recognized as blue colored bead and presents with red circles in the figure. This target is located in the lower part of the 2nd generation cell group model and closer to the wall of petri dish in isolation. Higher level of convergence was achieved after 150 times trials with many time step jumps of convergence.

C. Recognition of the Targeted Single Cell Models for 3rd Generation Group

Fig. 9 shows 11th recognition results of 3rd generation cell group model. Fig. 9(a) is a photo of 3rd generation cell group model before recognition. Rapid progress toward decentralization and arbitrary was found after second re-charge of red colored beads into original cell group model. Constituent ration between the number of red and blue beads was clearly changed with increase of red beads. Fig. 9(b) is a photo after recognition. The position of the target cell model of blue colored bead is located at upper part of the 3rd generation cell group and closer to the wall of petri dish in isolation.

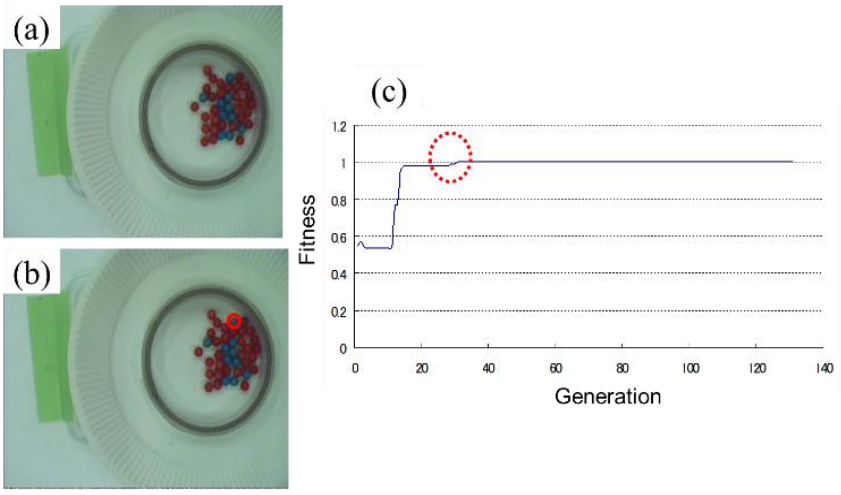

Fig. 9 The results of 11th recognition of the objected cell model in original cell group model: (a) Photo images of before, and (b) after recognition, and (c) convergence process of recognition

Fig. 9(c) shows the convergence process of fitness function F(Φ) with evolution cycles. Drastic convergence process step was observed at early evolutionary stage and high level of convergence was achieved before 40 times trials. Fig. 10 shows 16th recognition results of 3rd generation cell group model. Constituent ration between the number of red and blue beads was clearly changed with increase of red beads in Fig. 10(a). The targeted single cell model located in the middle of the group and set about with other red and blue colored beads. Fig. 10(c) shows the convergence process of fitness function F(Φ) with evolution cycles. There are many drastic convergence process steps were observed at every stage and higher level of convergence was achieved before 20 times trials.

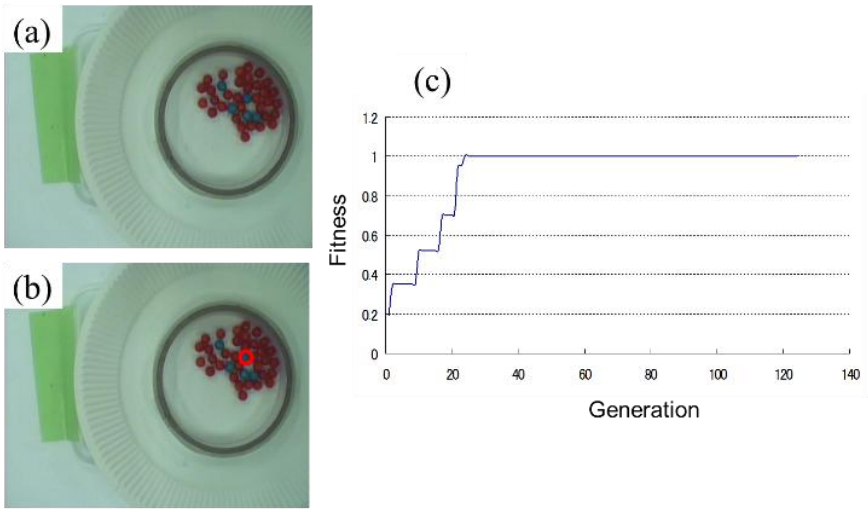

Fig. 10 The results of 16th recognition of the objected cell model in original cell group model: (a) Photo images of before, and (b) after recognition, and (c) convergence process of recognition

D. Recognition of the Targeted Single Cell Models for 4rd Generation Group

Fig.11 shows 18th recognition results of 4th generation cell group model. Fig. 11(a) is a photo of 3rd generation cell group model before recognition. Red colored beads almost owns about 98% of the 4th generation cell group model due to third re-charge of red colored beads and sortin in original cell group model. Fig.1 1(b) is a photo after recognition. The position of the target single cell model of blue colored bead is located at left side of the 4th generation cell group in isolation. Fig.11(c) shows the convergence process of fitness function F(Φ) with evolution cycles. There are many process steps observed at all stage and convergence level was beneath the case of 3rd generation model after 100 times trials. Fig. 12 shows 21th recognition results of 4th generation cell group model. It is found that removal of the target cell single models was completed and red colored breads took up all of space of 4th generation cell group model. Fig. 12(b) and (c) show 21th recognition results of 4th generation cell group model. The recognition of red colored beads was finished within 20 times convergence.

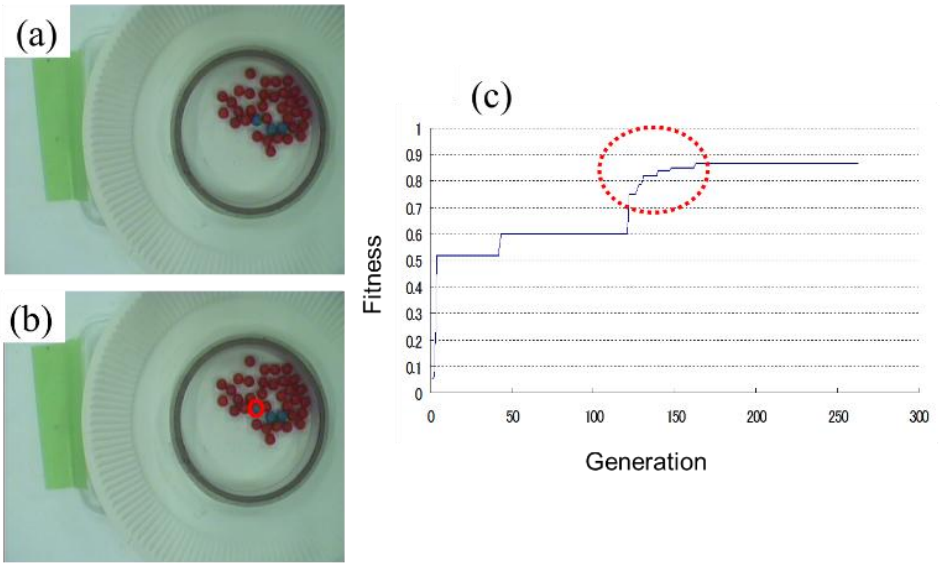

Fig. 11 The results of 18th recognition of the objected cell model in original cell group model: (a) Photo images of before, and (b) after recognition, and (c) convergence process of recognition

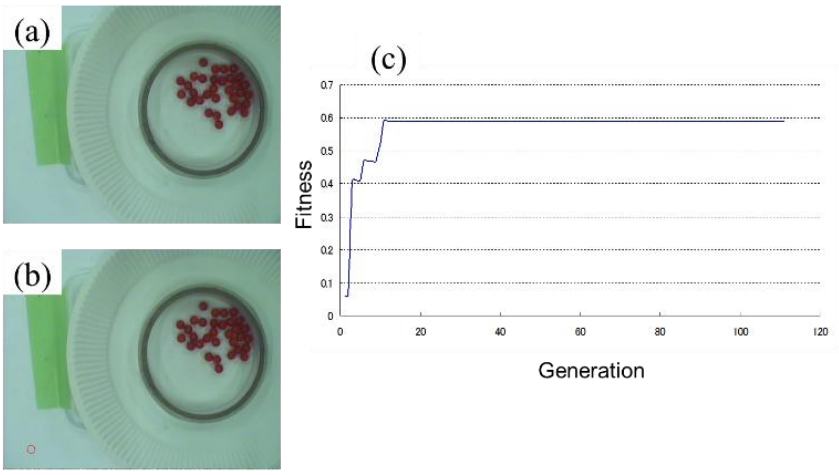

Fig. 12 The results of 21 th recognition of the objected cell model in original cell group model: (a) Photo images of before, and (b) after recognition, and (c) convergence process of recognition

E. Continuous Single Cell Sorting Process

Fig. 13 shows the change in number of red and blue beads in the cell group model through the trials. A blue bead was sorted correctly one robot motion and the number of blue bead monotonically decreased as trial proceeding. All of blue beads were removed from the generation cell group models completely after 20th sorting process. The number of red bead increased at 2nd, 3rd and 4th generation cell group models with adding red beads into these groups. From these results, it is clear that perfect sorting of targeted single cell model can be achieved from cell group model by using high-accuracy sorting hand system.

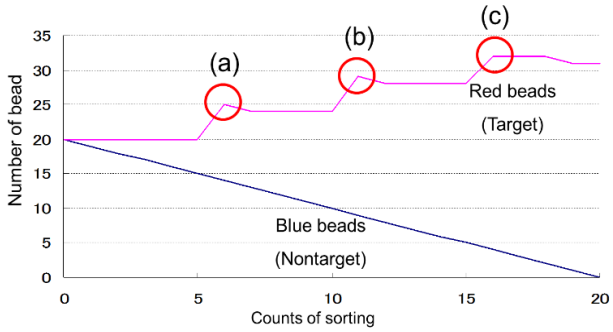

Fig. 13 The change in number of red and blue beads; Sorting errors occurred at the points of (a-c)

V. DISCUSSION

A. Single Cell Target Sorting from Cell Group Model

Single cell target sorting from original to 4th generation cell group models was conducted by the MOS robot.

Fig. 14 shows sorting situation of the targeted single cell model of blue colored bead from original cell group model by the bar hand. It is found that the MOS robot moved the bar hand over the target cell model (Fig. 14(a)) and sorted the single cell target in a accurately-predicted manner (Fig. 14(b)).

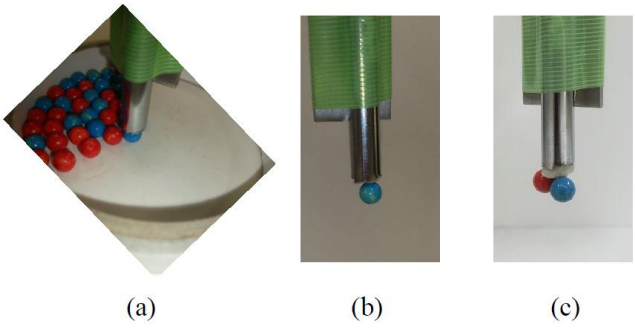

Fig. 14 Sorting of targeted cell model by MOS robot; (a) and (b) Sorting of targeted cell model (blue) and (c) Sorting of targeted and unintended cell models

B. Single Cell Target Recognition and Sorting Speed of Sorting Process by MOS Robot

Fig. 15 shows the recognition time at every sorting process. Convergence speed is 5 sec per 100 generation and the recognition time was obtained by convergent cycle and its speed. It is clear that the recognition action of the targeted single cell by MOS robot finished within 13 sec and sorting operation required 2-3 sec afterword. Therefore, it is concluded that total sorting time of single cell target from the cell group model finished within 15-16 sec.

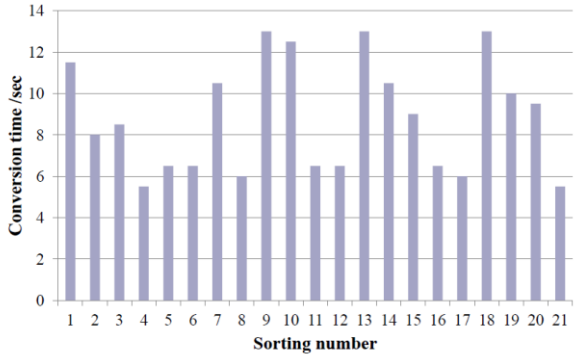

Fig.15 Conversion time as a function of sorting number

Fig. 15 Conversion time as a function of sorting number

C. Sorting Error of Single Cell Target from Cell Group Model

The MOS robot very often picked up over two of single nontarget cell and single target iPS cell at a time, as shown in Fig. 14(c). Three times selection error occurred in selection process and was indicated by arrows in Fig. 13. Red and blue beads were picked up in the chaotic aftermath of change of generation for cell group model. Fig. 16 shows the change in the maximum goodness of fitness at selection trials. Each error case occurred at the beginning of increase phase of goodness of fitness change. Comparing with conversion process between normal and error selection processes as shown in Fig. 5(c) and Fig. 7(c), Fig. 9(c) and Fig. 11(c), normal process behaves in a staircase pattern, whereas the error process inches toward increase just before convergence. In error cases, the target cell models are surrounded with other cell models with lower population. From these facts, it is indicated that the MOS robot took false recognition based on misinterpretation of local maximum or minimum value in Ω region as globally-optimized F(Φ), above-mentioned in section 2.1. Here, recognition depth at normal and error cases of single cell sorting were investigated.

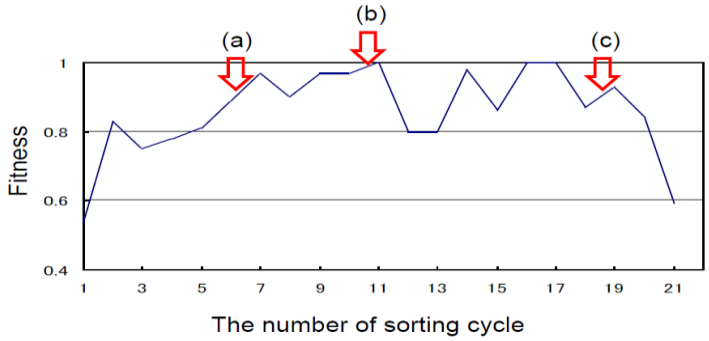

Fig 16 The change in fitness as a function of the number of sorting cycle; Sorting errors occurred at pointed of (a)-(c)

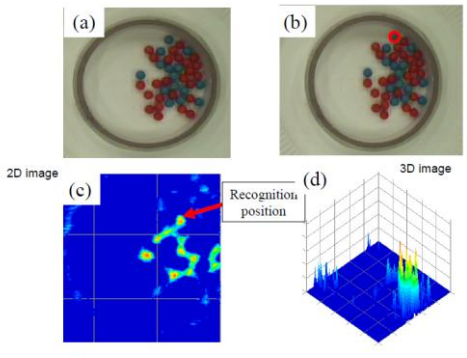

Fig. 19 The 6th circuit recognition and position of the single cell target of blue colored bead from red and blue mixture cell group model: Before (a) and after recognition (b), position(c) and recognition depth (d)

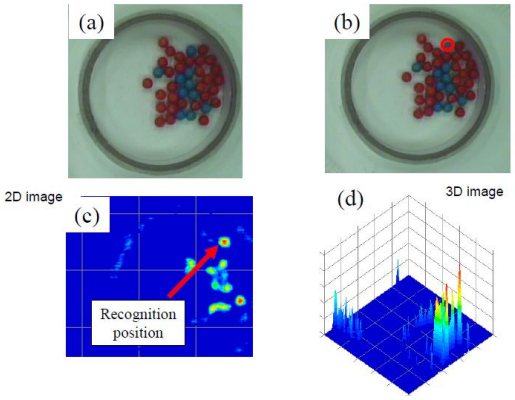

Fig. 20 The 11th circuit recognition and position of the single cell target of blue colored bead from red and blue mixture cell group model: Before(a) and after recognition(b), position(c) and recognition depth (d)

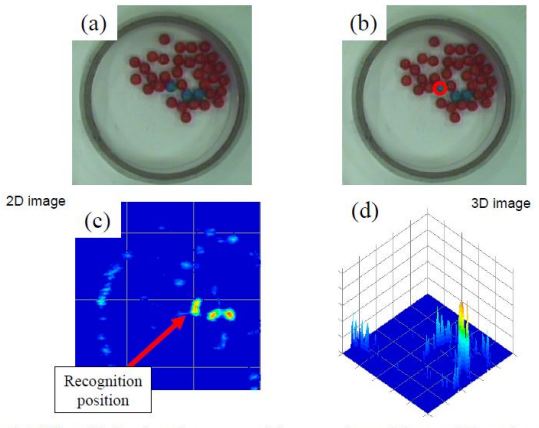

Fig. 21 The 18th circuit recognition and position of the single cell target of blue colored bead from red and blue mixture cell group model: Before(a) and after recognition(b), position(c) and recognition depth (d)

D. Simultaneous Recognition of Multiple Cell Targets by MOS

In practical use of MOS controlled robot for cell sorting, very high recognition and sorting speeds are required and simultaneous recognition of multiple cell target was conducted with cell group models. **Figs.22 and 23** show peaks of fitness for blue cell targets in red cell group. These data were obtained in the condition of 100 convergence process of recognition within 0.001 variation by GA. There are multiple peaks of recognition corresponding to the position of blue collared cell models in cell group and fitness value of these peaks in Fig. 22 are over 0.4, of which is enough to be recognized and sorted by multiple hand MOS robots.

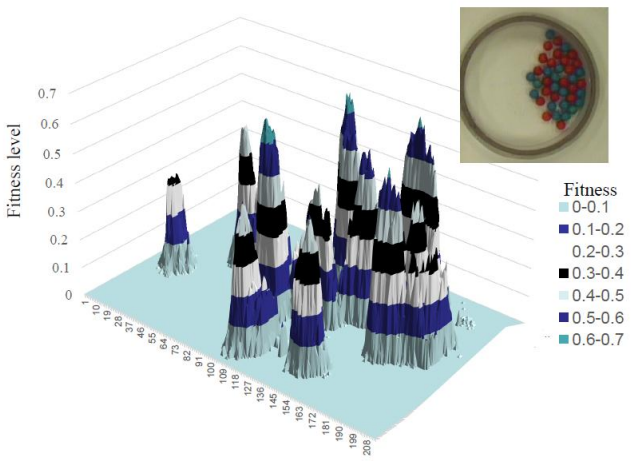

Fig. 22 Simultaneous GA recognition of multiple targeted cell in cell group

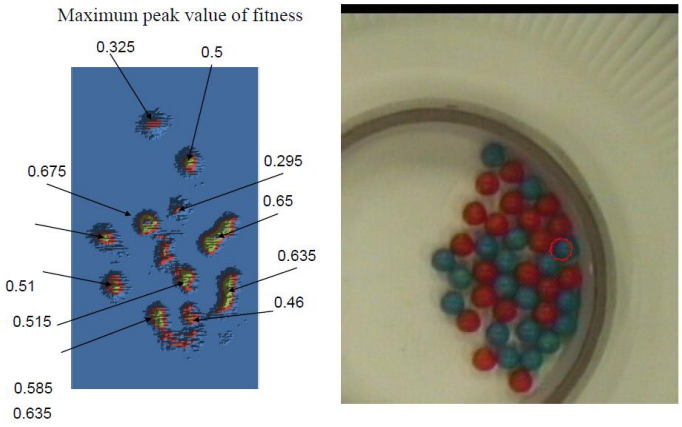

Fig. 23 Fitness distribution of the targeted cells (blue collared) recognized by MOS

E. The Concept of MOS Controlled Cell Sorting System

From these results, it can be concluded that perfect sorting of multiple targeted cells can be achieved from cell group by high-speed and accuracy sorting hand system by MOS control and the concept of MOS controlled cell sorting system was shown in Fig. 24. Here, binocular microscope MOS controlled robot is adopted to upgrade micro ordered handling for 10-30 μ m targeted cells. Binocular scoping of targeted cell guarantees precise x, y and especially z position of cells in culture vessel and improve high-accuracy sorting of the targeted cells. Under the MOS recognition of shape and position of stained targeted cells (red collared), MOS robot controls the micro magnet values directly above the targeted cells and sorting to another extraction vessel. Repetition of this extractive process improves purity of sorting cells.

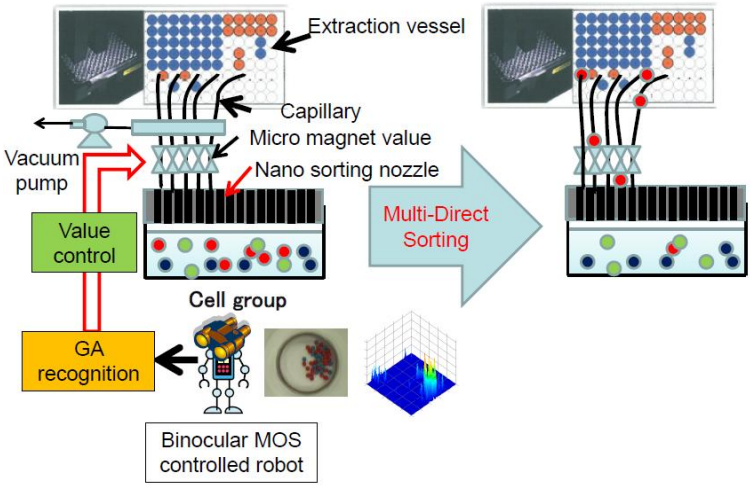

Fig. 24 Single and group cell sorting process

VI. CONCLUSIONS

A new control scheme "Move on Sensing" technology has been proposed and demonstrated its great potential as an autonomous control system to culture target iPS cells into objective organs, with which lost organs by curative operations can be replaced. To obtain curative organs and tissues, sorting operation of the target cell from indifferent cells is inevitable and a huge amount of sorting works is requested. For this presumable requirement to treatment using iPS, the proposed MOS robot control strategies robots have been confirmed to be able to have premising role in medical treatments for regeneration medicine.

In this paper, cell growing simulation was conducted using the visual servoing robot system and the following results were derived:

(1) Remove of the targeted cell models is completed by 20 times selection process from original cell group model composed of 20 red and 20 blue collared beads.

(2) Double pick-up error of red and blue beads occurred at only three times in all selection process. Sorting process was subjected to error at increasing of cell model, but it derives from accuracy of sorting hand and not recognition process on MOS technology.

(3) High-accuracy sorting operation of iPS cell model was achieved.

(4) Retrievability of the discrete cell models isolated from group model is ensured by use of the MOS control.

(5) From these performances of MOS control robots, MOS control cell sorting system was proposed in present study.

REFERENCES

[1] K. Takahashi and S. Yamanaka, "Induction of pluripotent stem cells from mouse embryonic and adult fibroblast cultures by defined factors," Cell, vol. 126, no. 4, pp.663-676, 2006.

[2] H. Zhou, S. Wu, J. Y. Joo, and et al.,"Generation of Induced Pluripotent Stem Cells Using Recombinant Proteins," Cell Stem Cell, vol. 4, no. 5, pp. 381-384, 2009.

[3] K. Okita, T. Ichisaka, and S. Yamanaka, "Generation of germline-competent induced pluripotent stem cells," Nature, vol. 448, no. 7151, pp. 313-317, 2007.

[4] M. Wernig, A. Meissner, R. Foreman, T. Brambrink, M. Ku, K. Hochedlinger, B. E. Bernstein, and R. Jaenisch, "In vitro reprogramming of fibroblasts into a pluripotent ES-cell-like state," Nature, vol. 448, no. 7151, pp. 318-324, 2007.

[5] N. Maherali, et al., "Directly reprogrammed fibroblasts show global epigenetic remodeling and widespread tissue contribution," Cell Stem Cell, vol. 1, no. 1, pp. 55-70, 2007.

[6] S. Hutchinson, G. Hager, and P. Corke, "A Tutorial on Visual Servo Control," IEEE Transactions on Robotics and Automation, vol. 12, no. 5, pp. 651-670, 1996.

[7] F. Chaumette, and S. Hutchinson, "Visual Servo Control, Part 1: Basic Approaches," IEEE Robotics and Automation Magazine, pp. 82-90, Dec. 2006.

[8] G. Chesi, K. Hashimoto, D. Prattichizzo, and A. Vicino, "Keeping features in the field of view in eye-in-hand visual servoing:A switching approach," IEEE Transactions on Robotics, vol. 20, Iss. 5, pp. 908-914, 2004.

[9] M. Minami, J. Agbanhan, and T. Asakura, "Robust Scene Recognition using a GA and Real-world Raw-image," Measurement,Elsevier, vol. 29, pp. 249-267, 2001.

[10] J. Zhu, Y. Mae, and M. Minami, "Finding and Quantitative Evaluation of Minute Flaws on Metal Surface Using Hairline," IEEE Transactions on Industrial Electronics, vol. 54, no. 3, pp. 1420-1429,2007.

[11] M. Minami and W. Song, "Hand-eye-motion Invariant Pose Estimation with On-line 1-step GA -3D Pose Tracking Accuracy Evaluation in Dynamic Hand-eye Oscillation-," Journal of Robotics and Mechatronics, vol. 21, no. 6, pp. 709-719, 2009.

[12] H. Suzuki and M. Minami, "Visual Servoing to catch fish Using Global/local GA Search," IEEE/ASME Transactions on Mechatronics, vol. 10, no. 3, pp. 352-357, 2005.

[13] W. Song, Y. Fujia, and M. Minami, "3D Visual Servoing by Feedforward Evolutionary Recognition," Journal of Advanced Mechanical Design, Systems, and Manufacturing (JSME), vol. 4, no. 4, pp. 739-755, 2010.

[14] M. Sakawa, "Optemaization of non-linear systems," Akaskura shoten, 2010.

[15] M. Fukushima, "Fundemental study of optemaization of non-lenar systems," Akaskura shoten, 2010.